Multifrequency High-Field EPR Study of the Interaction between the Tyrosyl Z Radical and the Manganese Cluster in Plant Photosystem II

Pierre Dorlet, Alain Boussac, A. William Rutherford, and Sun Un*

Section de Bioénergétique, Département de Biologie Cellulaire et Moléculaire, CNRS URA 2096, Bât. 532, CEA Saclay, F-91191 Gif-sur-Yvette Cedex, France

Received: July 26, 1999; In Final Form: October 1, 1999

The light-driven oxidation of water to dioxygen is catalyzed by the enzyme photosystem II. A four-manganese ion cluster and a tyrosine, Y_Z, are present in the catalytic site. In preparations inhibited by addition of acetate or removal of the calcium cofactor, it is possible to trap the tyrosyl radical in interaction with the metal cluster. The coupled species is characterized by a broad split EPR signal at 9 GHz. In this work, high-field EPR has been used for further characterization of the coupling. The 285, 190 and 95 GHz EPR spectra of the interacting system are reported. Analysis of these spectra yielded exchange and dipolar couplings of the same magnitude as those found with 9 GHz EPR. However, the high-field spectra show that the coupling between the radical and the manganese cluster has opposite sign in acetate-treated compared to calcium-depleted samples. The sign difference indicates differences in the electronic structure of the radical−metal center pair. Comparisons are made between photosystem II and other enzymes containing radicals interacting with metal centers. Possible explanations for the difference in sign are proposed. The difficulty in obtaining reliable structural information for the spin coupled system is addressed.

Introduction

The photosynthetic oxidation of water to oxygen occurs in photosystem II (PS II), an enzyme found in green plants and cyanobacteria.[1] During the catalytic cycle, photon absorption by chlorophylls induces electron transfer that leads to the storage of oxidizing equivalents in the oxygen evolving complex which comprises a cluster of four manganese ions and a redox-active tyrosine Y_Z. A mechanism invoking $Y_Z^{\bullet}$-mediated hydrogen atom abstraction from substrate water bound to the metal cluster has been proposed.[2] Four equivalents are needed before two molecules of water can be oxidized and molecular oxygen released. The intermediate states in the catalytic cycle are called the S_n states where n varies from 0 to 4 and denotes the overall oxidation state of the oxygen evolving complex.[3]

In the S_2 state, the manganese cluster has an effective spin $S = 1/2$ and exhibits an EPR signal known as the multiline signal.[4] Two inorganic cofactors, Ca^{2+} and Cl^-, are required for the enzyme to function normally. In preparations depleted of either of these cofactors water oxidation is inhibited.[5] In several of these depleted preparations the usual S_2 to S_3 transition is blocked, and illumination at 273 K results in the accumulation of a characteristic state. This state exhibits a broad split EPR signal arising from the magnetic interaction between an organic radical and the paramagnetic manganese cluster in a formal S_2 state.[6] This state, sometimes referred to as a modified S_3 state or $S_2rad^{\bullet}$ state, was first reported in PS II preparations which were depleted of the calcium cofactor.[6]

Addition of high concentrations of acetate to a sample also inhibits PS II and allows the trapping of the broad split EPR signal assumed to arise from the same state.[7] Acetate is supposed to inhibit oxygen evolution by replacing the chloride cofactor.[8] The width of the splitting which relates to the strength of the magnetic interaction varies between different types of preparations, ranging from about 9 mT to 23 mT.[6,7,9] The nature of the radical involved in the interaction has been under debate for a long time. There was agreement that the radical arose from an amino acid residue, either histidine or tyrosine.[5(a),10−12] By using electron spin−echo envelope modulation in conjunction with specifically ^{2}H-labeled tyrosine in acetate-treated cyanobacteria PS II mutants the radical was identified as being $Y_Z^{\bullet}$.[13] The state in which it interacts with the manganese cluster is now referred to as $S_2Y_Z^{\bullet}$. In the native oxygen evolving system it is not possible to trap $Y_Z^{\bullet}$ in the presence of the metal cluster because of the rapid reduction of the radical by the metal center.

A number of EPR studies and simulations have been done on this signal in part to determine the nature of the coupling. In calcium-depleted preparations, Boussac and co-workers simulated the EPR split signal assuming a weak exchange interaction between the metal cluster and the radical.[10] In the same way, MacLachlan and co-workers simulated the signal arising from calcium-depleted material as well as sodium acetate, calcium acetate, and ammonium chloride treated samples.[14] The spectral features for all of the different types of preparations could be simulated with a weak exchange interaction between the two species. Britt and co-workers simulated electron magnetic resonance data by modeling the interaction as dipolar coupling[12,15] (and assuming an $S = 1$ state for the cluster in ref 12). On the basis of new ^{55}Mn ENDOR data they published new simulations with dominant exchange interaction between two $S = 1/2$ spins.[1] Other recent simulations[17,18] based on a model including both dipolar and exchange terms for the signal obtained in acetate-treated preparations showed that the interaction was predominantly of the exchange type with an antiferromagnetic coupling of −800 to −850 MHz and a dipole−dipole contribution of −140 to −170 MHz.

* Corresponding author. E-mail: sun@ozias.saclay.cea.fr.

10.1021/jp992420k CCC: $18.00
Published on Web 11/18/1999

In this work, the magnetic interaction between the two species was further studied by using high-field EPR spectroscopy. The spectra of the coupled system were obtained at several frequencies in the range 95−285 GHz for acetate-treated PS II samples as well as Ca-depleted preparations, and the results were simulated and analyzed along with the 9 GHz data. In particular, it will be shown that the use of very high frequency allows the direct determination of the sign of the exchange interaction (ferromagnetic or antiferromagnetic interaction).

Experimental Section

Sample Preparation. All biochemical preparations were performed on ice under dim green light. Photosystem II membranes were prepared with the procedure described previously.[19] The preparations were frozen at a chlorophyll concentration of about 8 mg_{Chl}/mL in SMN buffer (sucrose 0.4 M, MES 50 mM, pH 6.0, NaCl 15 mM) and stored at −80 °C until used. Photosystem II reaction center cores were prepared by following the method developed by Mishra and Ghanotakis[20] except for the following modifications (Ghanotakis, personal communication). After incubation with octyl-β-D-thioglucopyranoside detergent the mixture was directly diluted in a 2:1 ratio with SMN buffer containing 30 mM $MgCl_2$ and further incubated for 5 min in the dark. The preparation was centrifuged at 20 000 rpm for 30 min. The supernatant was diluted in a 2:1 ratio with MN buffer (MES 50 mM, pH 6.0, NaCl 15 mM) and the cores pelleted by 40 min centrifugation at 20 000 rpm.

Acetate treatment was carried out by washing the preparation twice with SM buffer pH 5.5 containing 500 mM acetate and 100 mM calcium. In the case of cores, the treatment was done directly after the preparation. One washing was sufficient to induce the maximum $S_2Y_Z^\bullet$ signal in these more resolved preparations. After acetate treatment, samples were put directly in calibrated quartz EPR tubes along with 1 mM PPBQ as an electron acceptor (PPBQ was added from a stock solution in DMSO).

Calcium depletion was carried out by diluting PS II with SMN buffer down to a concentration of 1 mg_{Chl}/mL and adding an equal volume of SMN buffer containing 4 M of sodium chloride. The resulting mixture was incubated for 20 min under room light. EDTA was added to a final concentration of 1 mM and the solution further incubated in the dark for 5 min then centrifuged at 20 000 rpm for 20 min. The pellet was washed twice in SMN buffer.

Trapping of the $S_2Y_Z^\bullet$ state was performed by illuminating the sample at 273 K for 10 s followed by 15 s of additional illumination as the temperature was lowered to about 180 K in an ethanol bath cooled with liquid nitrogen. Dark adaptation to allow the decay of the $S_2Y_Z^\bullet$ state was done by incubating the sample at 193 K in complete darkness for 48 h. All samples were controlled with 9 GHz EPR for the presence of the $S_2Y_Z^\bullet$ signal and its complete disappearance upon dark adaptation.

EPR Spectroscopy. 9 GHz EPR spectra were recorded with a TE_{102} mode cavity at liquid helium temperatures on a Bruker ESR 200 spectrometer equipped with a liquid helium continuous flow cryostat and transfer line from Oxford Instruments. The microwave frequency was measured with a Hewlett-Packard 5350B frequency counter connected to the microwave bridge.

At 95 GHz and higher frequencies, EPR spectra were recorded on a lab-built transmission spectrometer whose principles are similar to those described by Muller and co-workers.[21] In this case, however, a Gunn diode microwave source capable of generating a maximum output power of 90 mW over a 90−100 GHz frequency range was used as the fundamental microwave source. The frequency was measured by using a frequency counter (EIP Microwave Inc., Milpitas, CA) with a better than 1 kHz accuracy. In conjunction with the Gunn oscillator, a frequency doubler and a frequency tripler (Radiometric Physics, Menkenheim, Germany) were used to work in the 180−200 GHz and 270−300 GHz frequency ranges, respectively. For simplicity in the text, we refer to the different bands as 9, 95, 190 and 285 GHz rather than the exact frequency. The signal was detected by using an In−Sb bolometer (QMC Instruments Ltd., London, England) in conjunction with a lock-in amplifier (SRS, Sunnyvale, CA) and field modulation. The amplitude of the modulation field was calibrated by using a standard sample. The magnetic field was generated by using a superconducting 10.5 T magnet (Oxford Instruments, Oxon, England). The value of the magnetic field was obtained from the magnet power supply which has a manufacturer specified accuracy of ±0.05 mT. Sample temperature regulation was achieved by using a built-in helium flow cryostat.

Spectral Simulations. Calculations were based on a spin-pair model by using the Hamiltonian of eq 1 (see following section). The powder spectra were obtained by calculating the resonant field for 100 000 random orientations of the applied magnetic field with respect to the *g*-axes frames and summing the results with their respective transition probability. The resulting orientation integrated spectrum was convoluted with a derivative Gaussian line shape with a suitable line width. The calculated spectrum was scaled to the experimental spectrum by using a scaling factor obtained from a linear fit of 10 to 20 data points. Variable parameters were estimated by minimizing the root-mean-square (rms) difference between the calculated and the experimental spectra. Nonlinear minimization was achieved by using standard simplex and conjugate gradient procedures.[22] The region containing the tyrosyl D radical signal was excluded from the rms calculation. It did not contribute to the minimization. All calculations were performed on a DEC Alphastation 250 (Maynard, MA) using local programs written in Fortran-77.

Theory

The theory of spin coupled systems has been discussed in detail.[23] In the following, we review the salient aspects of the problem involving a tyrosyl radical coupled to a four-manganese cluster with emphasis on the application of high magnetic fields. The spin Hamiltonian for such a coupled system is given by

$$\hat{H} = \beta\vec{\mathbf{B}}_0\tilde{\mathbf{g}}_{Tyr}\hat{\hat{\mathbf{S}}}_{Tyr} + \beta\vec{\mathbf{B}}_0\,\tilde{\mathbf{g}}_{Mn}\hat{\hat{\mathbf{S}}}_{Mn} + \sum_{i=1}^{4}\hat{\hat{\mathbf{I}}}_i\tilde{\mathbf{A}}_i\hat{\hat{\mathbf{S}}}_{Mn} + \hat{\hat{\mathbf{S}}}_{Tyr}\cdot\tilde{\mathbf{C}}\cdot\hat{\hat{\mathbf{S}}}_{Mn} \quad (1)$$

where the spin parameters g_{Tyr}, g_{Mn}, A_i and C are tensors and S and I are vector spin operators. The manganese cluster is in fact described by effective spin parameters and operators that describe the spin-$^1/_2$ ground state. The hyperfine term for the tyrosyl radical is neglected because the coupling constants[24] are considerably less than the line width of the signals studied. Each of the Zeeman terms, the first two terms of Eq. 1, are on the order of 3 (at 3.5 T) to 30 cm^{-1} (at 10 T) compared to 0.010 cm^{-1} for A and < 0.040 cm^{-1} for C. An important consequence of this is that the number of terms introduced by the hyperfine and spin-spin coupling Hamiltonians is very much reduced. In addition, if it is assumed that the tensors are collinear, eq 1 greatly simplifies to

$$\hat{H} = g_{\mathrm{Tyr}}\beta B_0\hat{S}_{\mathrm{TyrZ}} + (g_{\mathrm{Mn}}\beta B_0 + \sum_{i=1}^{4} A_i\hat{I}_{iZ})\hat{S}_{\mathrm{MnZ}} + C_{ZZ}\hat{S}_{\mathrm{TyrZ}}\hat{S}_{\mathrm{MnZ}} + C_{\pm}(\hat{S}_{\mathrm{Tyr}+}\hat{S}_{\mathrm{Mn}-} + \hat{S}_{\mathrm{Tyr}-}\hat{S}_{\mathrm{Mn}+}) \quad (2)$$

with

$$g = \sqrt{g = g_{\mathrm{X}}^2 \sin^2\chi\cos^2\psi + g_{\mathrm{Y}}^2\sin^2\chi\sin^2\psi + g_{\mathrm{Z}}^2\cos^2\chi}$$

and

$$Ai = \left(\sqrt{a_{i\mathrm{X}}^2\, g_{\mathrm{MnX}}^2 \sin^2\chi\cos^2\psi + a_{i\mathrm{Y}}^2\, g_{\mathrm{MnY}}^2 \sin^2\chi\sin^2\psi + a_{i\mathrm{Z}}^2\, g_{\mathrm{MnZ}}^2\cos^2\chi}\right)/g_{\mathrm{Mn}}^2$$

All of the spin parameters are scalar quantities. χ is the angle between the magnetic field and the g_Z axis and ψ is the angle between the projection of the magnetic field on the (g_X, g_Y) plane and the g_X axis. This Hamiltonian can be readily solved analytically. The results describe a four-level system, each level of which is further divided into 1296 hyperfine sublevels. The lowest energy manifold is that of the unperturbed $|\beta\beta\mathrm{M}>$ electronic spin state while the highest is that of the unperturbed $|\alpha\alpha\mathrm{M}>$. The inner two wavefunctions and their energies depend on the parameter Ω defined by $\sqrt{\delta^2+4C_{\pm}^2}$ where $\delta = g_{\mathrm{Tyr}}\beta B_0 - (g_{\mathrm{Mn}}\beta B_0 + \mathrm{mA})$ and $\mathrm{mA} = \sum_{I=5/2}^{5/2}\sum_{i=1}^{4} \mathrm{m}_{\mathrm{I}_i}\mathrm{A}_i$. The energies are given by $(-C_{zz} \pm 2\Omega)/4$. The wavefunctions are of the form $u\ |\alpha\beta\mathrm{M}> + v\ |\beta\alpha\mathrm{M}>$ where u and v are trigonometric coefficients determined by the ratio of δ and Ω and M describes the hyperfine states. For a single orientation of the magnetic field with respect to the common tensor axis system, the wavefunctions and energies will vary from spin-pair to spin-pair due to their dependence on the hyperfine states. This effect is not negligible. Even at 10 T, the magnitude of |mA| is comparable to the anisotropy in the Zeeman interaction and can dominate δ. As will be seen, it is also comparable to the coupling constants. Hence, the normal singlet−triplet nomenclature is not particularly useful.

An aspect of the four-level problem, especially relevant to HF-EPR, is the thermal population of the four spin states. For an applied field of 10 T, the energies of the allowed transitions from the lowest spin state are about 285 GHz. The corresponding temperature ($h\nu/k$) is 14 K. Therefore, for experiments carried out at 4 K, only the $|\beta\beta>$ state will be significantly populated. Hence, only two of the four allowed transitions will be observable, one attributable to the metal and the other to the radical in the absence of interaction. The energies of these transitions are respectively

$$\Delta E_{24} = \frac{1}{2}(g_{\mathrm{Tyr}}\beta B_0 + (g_{\mathrm{Mn}}\beta B_0 + \mathrm{mA}) + \Omega - C_{ZZ}) \quad (3)$$

$$\Delta E_{34} = \frac{1}{2}(g_{\mathrm{Tyr}}\beta B_0 + (g_{\mathrm{Mn}}\beta B_0 + \mathrm{mA}) - \Omega - C_{ZZ}) \quad (4)$$

In the absence of spin coupling energies, the transition energies reduce to $g_{\mathrm{Tyr}}\beta B_0$ and $g_{\mathrm{Mn}}\beta B_0 + \mathrm{mA}$, respectively. The sign of C_{zz} will determine whether the transition energy lies above or below the transition energies corresponding to the uncoupled spins system (see Scheme 1). Hence, a straightforward temperature dependence study will yield the sign of the coupling constant.

Up to this point, we have not specified the nature of the spin coupling. In this study we have chosen the simplest model. The isotropic component of the coupling C is attributed to Heisenberg exchange J. The anisotropic component is modeled by an axial dipolar coupling D.[25] It is important to note that the radical is coupled to four metal centers, and this has important consequences as pointed out by Bertrand et al.[26] The summation over the four couplings can be reduced to a single effective coupling in the following manner:

$$\hat{H}_{\mathrm{EX}} = -\sum_{i=1}^{4} J_i\hat{\mathbf{S}}_{\mathrm{Mn}i}\cdot\hat{\mathbf{S}}_{\mathrm{Tyr}} = -(\sum_{i=1}^{4} K_iJ_i)\hat{\mathbf{S}}_{\mathrm{Mn}}\cdot\hat{\mathbf{S}}_{\mathrm{Tyr}} = -J\hat{\mathbf{S}}_{\mathrm{Mn}}\cdot\hat{\mathbf{S}}_{\mathrm{Tyr}} \quad (5)$$

where K_i are weighting coefficients derived from the Wigner−Eckart theorem. Although the use of a single coupling constant greatly simplifies the problem, the sign of the effective constant no longer carries any physical meaning unless the K_i coefficients are known. Even when all four intrinsic couplings are antiferromagnetic (i.e., negative) the effective coupling can, in fact, be positive depending on the values of K_i. Moreover, the same arguments can also be applied to dipolar coupling.[26,27]

Finally, we point out an approximation based on a physical interpretation of eq 2 which reduces the time required to calculate a spectrum. The tyrosyl radical experiences the magnetic field due to magnetic moment of the manganese cluster. This moment is largely determined by the applied magnetic field, but is modified by the internal hyperfine couplings within the cluster. The hyperfine contribution is due to four anisotropic hyperfine interactions arising from four spin-5/2 nuclei. A suitable approximation of the hyperfine contribution of the manganese cluster is a simple binomial distribution, the breath of which matches the multiline signal. Under this approximation, the multiline structure of the metal center will be lost. However, since the hyperfine interactions do not directly affect spin states of the radical, the calculated position and overall line shape of the tyrosyl radical portion of the spectrum will be unaffected compared to a complete calculation. Such an approximation has practical advantage in that the time required to calculate a spectrum is reduced since the summation over hyperfine states (1296 calculations) is replaced by a fixed function (<250 calculations).

Results

Position and Line Shape of the $S_2Y_Z^{\bullet}$ Signal. Figures 1 and 2 show the EPR spectra obtained for the Ca-depleted and acetate-treated PS II membrane preparations respectively in which the $S_2Y_Z^{\bullet}$ state was trapped. In all cases, the dark stable tyrosyl radical $Y_D^{\bullet}$ gives a strong EPR signal that overlaps with the signals studied in this paper. In the Ca-depleted samples, the 9 GHz spectrum shows the signal split by 14.5 mT peak to trough. In acetate-treated membranes, the 9 GHz spectrum shows two major features split by 23 mT accompanied by two satellite peaks split by 44 mT and an underlying multiline signal. These correspond to the usual spectra reported for these preparations. The other spectra in the figures show the high-field spectra obtained on the same sample.

For the Ca-depleted sample, at 285 GHz a single broad feature appears centered about 9 mT upfield from the $Y_D^{\bullet}$ g_z edge. At 190 and 95 GHz a similar signal is observed upfield from the $Y_D^{\bullet}$ signal. Downfield from the $Y_D^{\bullet}$ signal, there appears to be additional features just above the noise level. The spectra at high field for the acetate-treated sample are strikingly different from the corresponding spectra in Ca-depleted preparations. Most of the signal appears downfield from the $Y_D^{\bullet}$ signal. At 285 GHz, the main broad feature is centered about 20 mT from the g_x edge of the $Y_D^{\bullet}$ signal on the low field side. At 190 GHz

SCHEME 1. Stick Spectra for the Coupled System Showing the Position of the Transitions Depending on the Sign of the Interaction and the Effect of the Boltzmann Distribution[a]

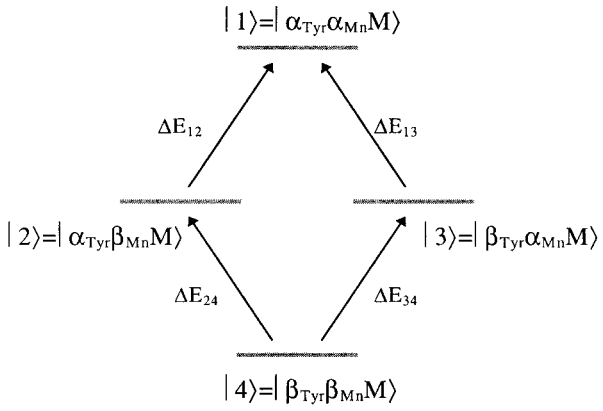

$$\Delta E_{24} = \frac{1}{2}\left(g_{Tyr}\beta B_0 + (g_{Mn}\beta B_0 + mA) + \Omega - C_{ZZ}\right)$$

$$\Delta E_{13} = \frac{1}{2}\left(g_{Tyr}\beta B_0 + (g_{Mn}\beta B_0 + mA) + \Omega + C_{ZZ}\right)$$

$$\Delta E_{34} = \frac{1}{2}\left(g_{Tyr}\beta B_0 + (g_{Mn}\beta B_0 + mA) - \Omega - C_{ZZ}\right)$$

$$\Delta E_{12} = \frac{1}{2}\left(g_{Tyr}\beta B_0 + (g_{Mn}\beta B_0 + mA) - \Omega + C_{ZZ}\right)$$

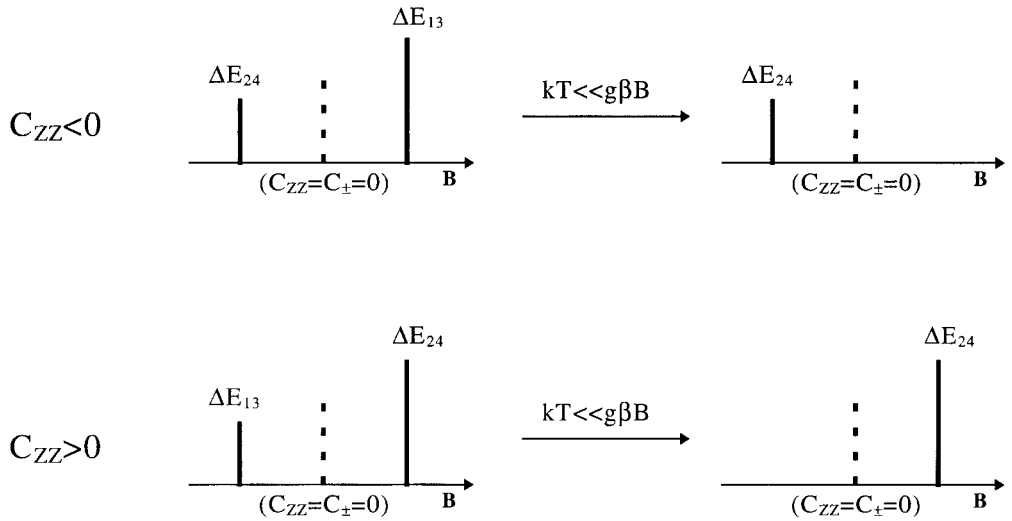

[a] Only the two transitions corresponding predominantly to the tyrosyl radical are represented. The same analysis applies to the other two allowed transitions not shown.

two peaks can be seen centered about 20 and 10 mT from the $Y_D^\bullet$ g_x edge on the low field side. A third peak is visible 9 mT upfield from the g_z edge of the $Y_D^\bullet$ signal. At 95 GHz, a broad signal appears on each side of the $Y_D^\bullet$ spectrum. Three of the six sharp lines from Mn(II) are also observed in this spectrum. The Mn(II) signal is absent at 190 and 285 GHz due to thermal depopulation at the temperature used to record the spectra. The 9 and 285 GHz EPR spectra of $S_2Y_Z^\bullet$ in acetate-treated reaction center cores are shown in Figure 3. For this preparation the splitting between the main features of the $S_2Y_Z^\bullet$ signal at 9 GHz is 21 mT, narrower than in membranes and reflecting a somewhat weaker interaction. At 285 GHz, the signal visible on the low-field side of the $Y_D^\bullet$ signal is centered about 15 mT from the g_x edge of the $Y_D^\bullet$ signal (Figure 3, right spectrum), in closer proximity than in membranes (Figure 2, spectrum 1).

All of these features reproducibly appeared in the high-field spectra for different samples of each preparation exhibiting the well-known "split signal" at 9 GHz. Upon dark adaptation at 193 K (see Experimental Section) the features completely disappeared and it was possible to reinduce them by reilluminating the sample at 273 K. We attribute these features to the signal arising from the magnetic interaction between the $Y_Z^\bullet$ radical and the manganese cluster. The field position and the extent of the $S_2Y_Z^\bullet$ signal were reproducible for several samples of a given type of preparation. Possible contaminating signals can be readily distinguishable by their *g*-values which can be resolved by high-field EPR. We observed no evidence of chlorophyll signals. They are narrow even at high fields and occupy the region between 2.0022 and 2.0035. No signals from cytochrome b_{559} are expected in the magnetic field regions of

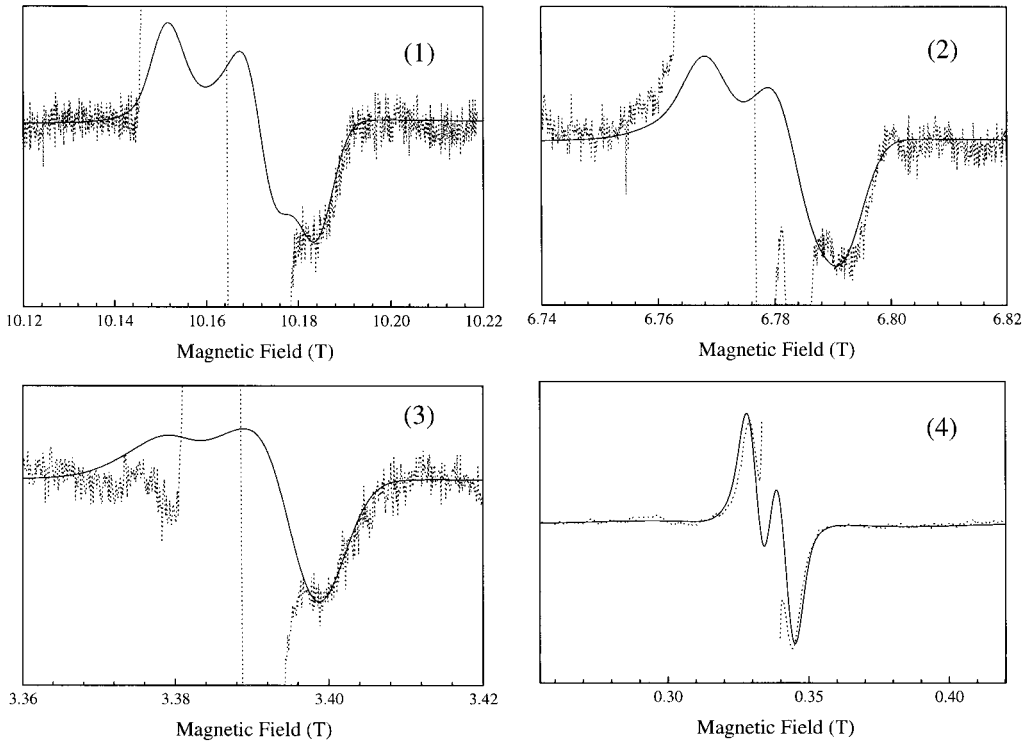

Figure 1. EPR spectra of the $S_2Y_Z^{\bullet}$ state in Ca-depleted PS II membranes at different frequencies. Experimental spectra are represented by dotted lines. Simulated spectra are superimposed as solid lines. Experimental conditions: (1) microwave frequency $\nu_{mw} = 285.1383$ GHz, modulation amplitude 2 mT, modulation frequency 3332 Hz, temperature T 4.2 K, time constant 300 ms; (2) microwave frequency $\nu_{mw} = 190.1634$ GHz, modulation amplitude 1.5 mT, modulation frequency 3332 Hz, T 4.2 K, time constant 1 s; (3) microwave frequency $\nu_{mw} = 95.0315$ GHz, modulation amplitude 2 mT, modulation frequency 3332 Hz, T 4.2 K, time constant 300 ms; (4) microwave frequency $\nu_{mw} = 9.43305$ GHz, modulation amplitude 1.5 mT, modulation frequency 100 kHz, T 10 K, time constant 20 ms. For simulation parameters see text and Table 1.

interest. The details of the line shape of the $S_2Y_Z^{\bullet}$ signal could, however, be affected by the distortion of the baseline due to microwave power saturation of the $Y_D^{\bullet}$ signal (see for example Figure 4 in the case of the acetate-treated sample). $Y_D^{\bullet}$ was found to saturate more readily than the $S_2Y_Z^{\bullet}$ state. The saturation properties (and therefore the distortion) of the $Y_D^{\bullet}$ signal depends on its interactions with the different paramagnetic cofactors present in the sample.[28] As a consequence, it was not possible to obtain light minus dark-adapted difference spectra because the line shape of $Y_D^{\bullet}$ is different for the two states of the samples. Figure 4 shows two examples of full scale spectra: the 190 GHz EPR spectra from acetate-treated membranes and the 285 GHz EPR spectra from Ca-depleted preparations after illumination to trap $S_2Y_Z^{\bullet}$ and after dark-adaptation. The spectral features attributable to $S_2Y_Z^{\bullet}$ are clearly distinguishable even on this scale.

Determination of the Coupling Parameters. To estimate quantitatively the coupling parameters, we simulated the experimental spectra. The g-values for the tyrosyl radical were taken from 285 GHz EPR spectra of $Y_D^{\bullet}$[29] and fixed. We assume no change in the g-values of the radical, although the proximity of the manganese cluster could modify them through electrostatic effects.[30] The g-values and the hyperfine couplings for the manganese cluster are not known accurately. As a starting point, the hyperfine interaction was modeled by a binomial distribution function (see Theory). This function was chosen to match the shape and extent of the multiline signal observed in the S_2 state of untreated preparations. Simulations using this approximation were nearly identical to those calculated by using the full hyperfine Hamiltonian. This demonstrated that the portions of the simulated spectra which are predominantly from the radical were insensitive to the details of the hyperfine couplings. As expected the g-values of the cluster had a much greater effect on the simulated spectra at high field (see next section). However, we started by keeping them constant and the adjustable parameters were J, D, and the two angles θ and φ defining the orientation of the axis joining the two dipoles in the g-axes frame. At 9 GHz the angles θ and φ have negligible effect on the overall line shape of the spectra but their impact on the simulated spectra increases with the frequency. The angles were determined by visual inspection of the simulated spectra at high frequency. The 190 GHz spectra obtained in acetate-treated samples was particularly useful for this work because it exhibits visible features arising from the splitting of all three g components of the tyrosyl signal (see Figure 4, right spectra).

The best fits obtained are shown in Figures 1, 2, and 3 along with the experimental spectra. In Ca-depleted preparations, the values for the couplings are $J = -0.42$ GHz and $D = -0.1$ GHz. The negative sign of J indicates that the tyrosyl radical and the manganese cluster are antiferromagnetically coupled. In acetate-treated PS II membranes, the values obtained are $J = 0.82$ GHz and $D = -0.12$ GHz. The two spins in this case are ferromagnetically coupled. As mentioned above for acetate-treated samples, the coupling is weaker in reaction center cores compare to membranes. Nonetheless, the high field data show that the coupling remains ferromagnetic in cores. The values obtained for cores are $J = 0.66$ GHz and $D = -0.11$ GHz.

In acetate-treated preparations variations in the splitting of the signal are observed at 9 GHz depending on whether the treatment is performed on cores or membranes. These variations are also observed at high field. In the case of Ca-depleted preparations, different size splittings are also observed for the signal at 9 GHz depending on the exact protocol used to prepare

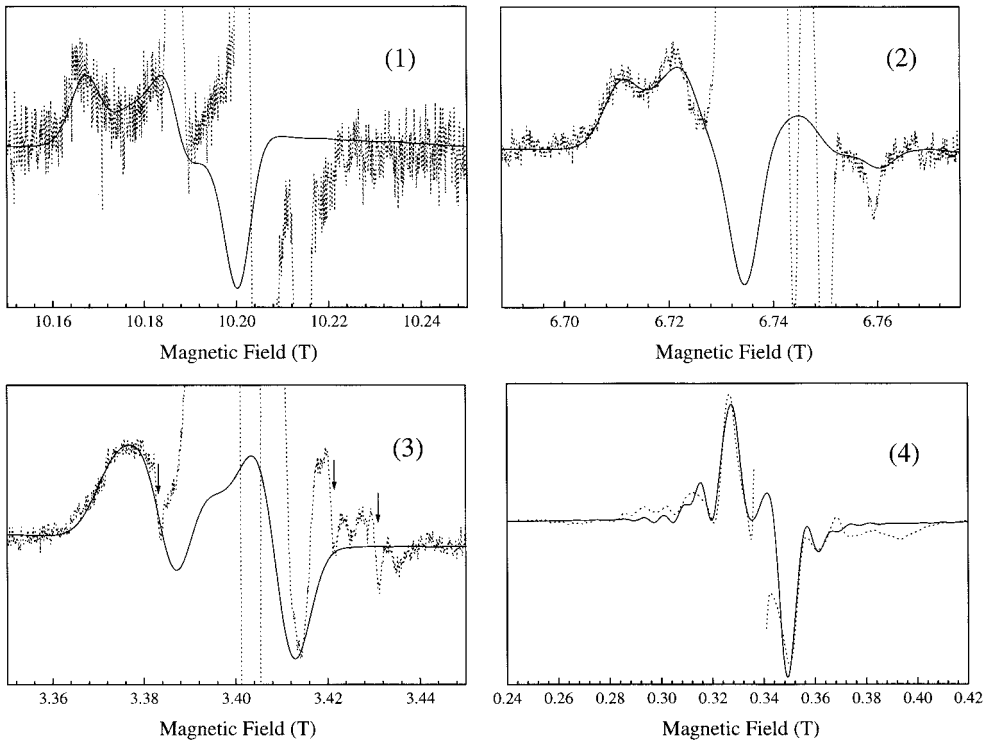

Figure 2. EPR spectra of the $S_2Y_Z^{\bullet}$ state in acetate-treated PS II membranes at different frequencies. Experimental spectra are represented by dotted lines. Simulated spectra are superimposed as solid lines. Experimental conditions: (1) microwave frequency $\nu_{mw} = 286.2321$ GHz, modulation amplitude 2 mT, modulation frequency 3318 Hz, T 2.5 K, time constant 300 ms; (2) microwave frequency $\nu_{mw} = 189.1418$ GHz; modulation amplitude 2 mT; modulation frequency 3318 Hz, T 3 K; time constant 1 s; (3) microwave frequency $\nu_{mw} = 95.3559$ GHz, modulation amplitude 1.5 mT, modulation frequency 3332 Hz, T 3 K, time constant 1 s, the sharp features indicated by arrows in the experimental spectrum are three of the six hyperfine lines from contaminating Mn(II); (4) microwave frequency $\nu_{mw} = 9.4677$ GHz, modulation amplitude 1.27 mT, modulation frequency 100 kHz, T 10 K, time constant 41 ms. For simulation parameters see text and Table 1.

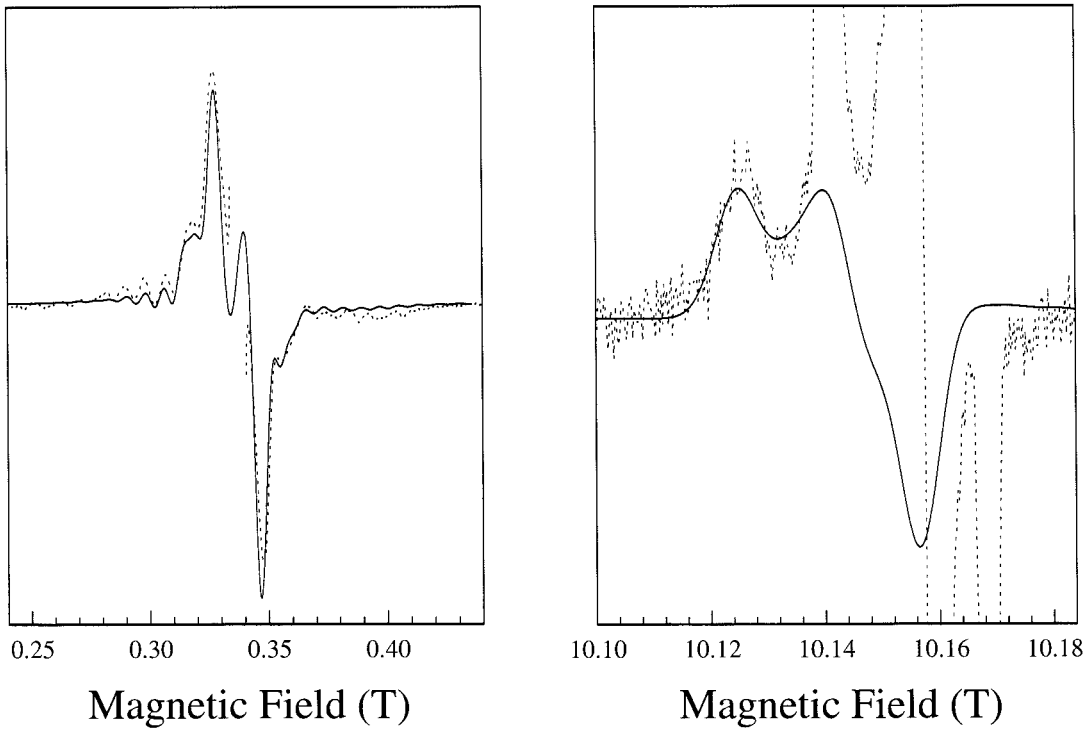

Figure 3. EPR spectra of the $S_2Y_Z^{\bullet}$ state in acetate-treated reaction center cores at X band (left panel) and 285 GHz (right panel). Experimental spectra are shown as dotted lines. Simulated spectra are superimposed as solid lines. Experimental conditions: (left panel) microwave frequency $\nu_{mw} = 9.464$ GHz, modulation amplitude 2 mT, modulation frequency 100 kHz, T 7 K, time constant 80 ms; (right panel) microwave frequency $\nu_{mw} = 284.9361$ GHz, modulation amplitude 2 mT, modulation frequency 3318 Hz, T 3.5 K, time constant 300 ms. For simulation parameters see text and Table 1.

the samples and on the presence or absence of the 17 and 23 kDa extrinsinc polypeptides that bind on the donor side of the protein. In this case, the variation of splitting at 9 GHz did not translate into an observable shift in the position of the broad

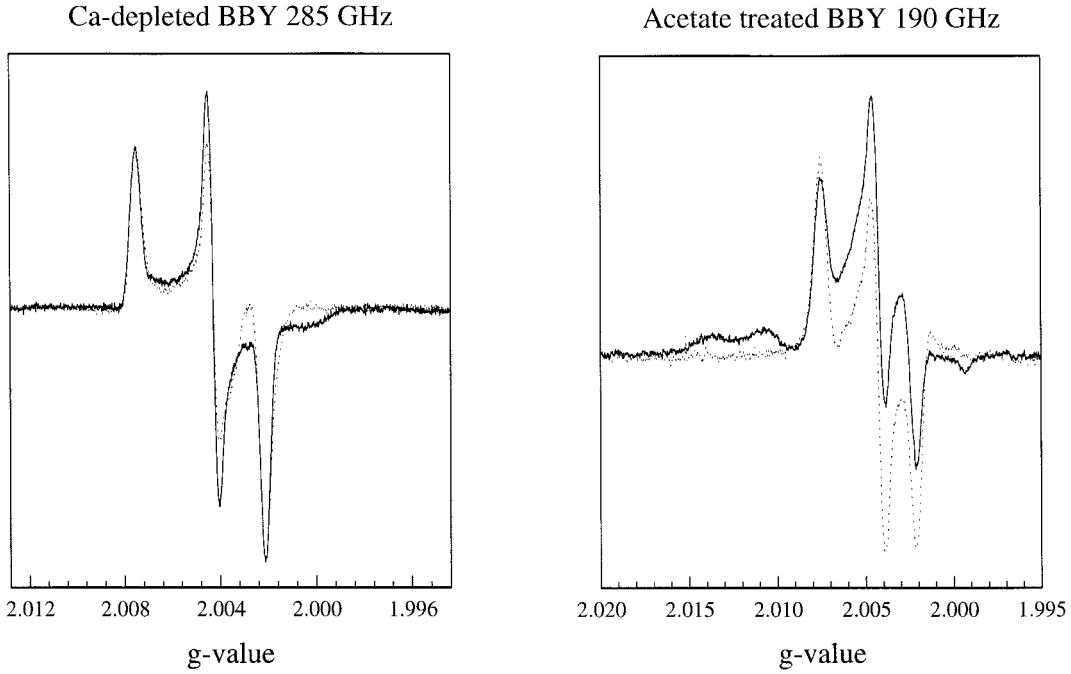

Figure 4. Two examples of full scale high-frequency EPR spectra in Ca-depleted and acetate-treated PS II membranes. Spectra shown as solid lines were recorded on samples in which the $S_2Y_Z^\bullet$ state was trapped; spectra shown as dotted lines were recorded on the same samples after dark adaptation. Experimental conditions: left panel, same as Figure 1 spectrum (1); right panel, same as Figure 2 spectrum (2).

TABLE 1: Parameters Used in the Simulations of the EPR Signals

Tyrosyl Radical			
$g_x = 2.0075$	$g_y = 2.0043$	$g_z = 2.0021$	
Manganese Cluster			
$g_x = 1.9967$	$g_y = 1.9955$	$g_z = 1.9600$	
Acetate-Treated Samples			
$a_{1x} = a_{1y} = 180$ MHz	$a_{2x} = 270$ MHz	$a_{3x} = 270$ MHz	$a_{4x} = 270$ MHz
$a_{1z} = 260$ MHz	$a_{2y} = a_{2z} = 210$ MHz	$a_{3y} = a_{3z} = 200$ MHz	$a_{4y} = a_{4z} = 230$ MHz
Ca-Depleted Samples			
$a_{1iso} = 420$ MHz	$a_{2iso} = 210$ MHz	$a_{3iso} = 148$ MHz	$a_{4iso} = 136$ MHz
Interaction			
Acetate-Treated PS II Membranes			
$J = 820$ MHz ($\sigma_J = 40$ MHz)		$D = -120$ MHz	$\theta = 90°$; $\varphi = 0°$
Acetate-Treated Reaction Center Cores			
$J = 680$ MHz ($\sigma_J = 40$ MHz)		$D = -110$ MHz	$\theta = 90°$; $\varphi = 0°$
Ca-Depleted PS II Membranes			
$J = -420$ MHz ($\sigma_J = 150$ MHz)		$D = -100$ MHz	$\theta = 90°$; $\varphi = 0°$

signal at high field (data not shown). To obtain good fits at all frequencies for the Ca-depleted preparation it was necessary to use a distribution in the exchange coupling. The distribution was modeled by a Gaussian function with a full width of σ_J at half-height (see Table 1). Without distribution, the coupling constants determined by fitting the high-field spectra were too large to account for the 9 GHz spectrum of the Ca-depleted sample. The main effect of the distribution in the coupling observed in the simulated spectra was a narrowing of the peak-to-trough width of the signal at 9 GHz while the calculated high-field spectra were relatively unaffected. The position of the signal remained unchanged, and any changes in line shape were small. The values and distribution width for the coupling constants are given in Table 1. Finally, we note that parameters that we have obtained are also consistent with the 3 GHz EPR spectrum (of Ca-depleted material) (see Supporting Information).

Effects of the *g*-Values and Hyperfine Coupling of the Metal Cluster. The exact *g*-values for the cluster had a noticeable effect on the simulated spectra of the $S_2Y_Z^\bullet$ signal for high magnetic fields. Data obtained at several frequencies in the range 9−285 GHz provided considerable constraints on the simulations. Hence it was possible to allow the *g*-values of the cluster to vary and to obtain those that fit best. The values are reported in Table 1. It is interesting to note that they are close to axial symmetry.

Because the magnitude of the hyperfine couplings for the metal cluster is on the same order as the coupling parameters between the radical and the cluster, it is important that the hyperfine term be included in order to accurately describe the $S_2Y_Z^\bullet$ state. At 95 GHz and higher frequencies, the hyperfine couplings for the metal center stay unresolved and contribute in part to the broadening of the spectra. At 9 GHz however, as in the case of acetate-treated preparations, the $S_2Y_Z^\bullet$ state exhibits an underlying multiline signal. By modeling the hyperfine term with a binomial distribution, the envelope of this multiline signal was obtained but the multiline structure was lost (see Supporting Information). To reproduce the details of the line shape, the full calculations using actual hyperfine

values were required. All of the simulations presented in this work used the full hyperfine calculation. The values used are given in Table 1. For calcium-depleted preparations, the hyperfine values were chosen to account for the dark stable multiline observed in the S_2 state and taken from the literature.[10] In the case of the acetate-treated samples, we chose values to account for the underlying multiline signal present in the $S_2Y_Z^\bullet$ signal at 9 GHz. However, we note that this set of hyperfine values is not likely to be unique.

Discussion

The high-field spectra were recorded at a temperature of 4.2 K or lower corresponding to a maximum Boltzmann energy kT of 87.5 GHz. Therefore for spectra recorded at high frequency, only the ground state will be significantly populated and the transitions arising from higher energy Zeeman states will not be observed or will give a signal of small amplitude (see Scheme 1). We were unable to observe the transitions that are predominantly from the metal cluster presumably due to insufficient sensitivity. The signal arising from the manganese cluster is very broad and therefore very small in amplitude. The signals we see correspond to transitions which belong predominantly to the radical. As shown in the theoretical section, the position of the signal with respect to the $Y_D^\bullet$ spectrum (which models the noninteracting tyrosyl radical signal) directly determines the sign of the interaction. Therefore it is clear from the high-field spectra that the sign of the coupling between the radical and the cluster must be opposite in acetate-treated and calcium-depleted preparations. Since the isotropic exchange interaction was found to dominate the dipolar interaction this means that the radical and the cluster are ferromagnetically coupled in acetate-treated preparations and antiferromagnetically coupled in calcium-depleted samples.

A previous study using 9 and 33 GHz EPR found the exchange coupling to be antiferromagnetic in acetate-treated PS II membranes.[18] In this work, the authors assign the sign of the coupling by looking at details in the simulations of a 9 GHz spectrum of the $S_2Y_Z^\bullet$ signal. In our work, the sign of the coupling is determined directly from the 190 and 285 GHz experimental spectra. At high field, the sign of the exchange coupling has a dramatic effect. Signals are either present or absent and it is very clear that any set of parameters which uses an antiferromagnetic coupling fails in simulating the high-field data for acetate-treated samples. Our parameters yield good simultaneous fits of the data taken at the four different frequencies we use, as well as the Q-band data presented in ref 18 (see Supporting Information for calculated spectra with positive and negative values for J). This points to the strength of multifrequency high-field EPR over conventional-frequency EPR in characterizing the exchange coupling.

Although less common than antiferromagnetic coupling, cases of ferromagnetic coupling between a radical and a metallic center in a protein have been reported in the literature.[31−33] In cytochrome *c* peroxidase compound ES, a tryptophanyl radical is weakly coupled to an oxyferryl moiety. It has been shown[31] that the coupling is distributed and both ferromagnetic and antiferromagnetic components are present with $J \approx 2.94$ GHz for one-third of the enzyme population and $J \approx -1.47$ GHz for two-thirds of the enzyme population in the sample. The dual nature of the exchange coupling, ferromagnetic and antiferromagnetic, in the same given type of preparation has been explained by a bimodal conformational substate distribution (see below) of the protein in the frozen solution.[31] The difference in the sign of J in this case has been postulated to arise from differences in orbital overlaps on the exchange path between the Trp$^\bullet$ radical and the heme due to distribution in the protein conformation. In PS II both ferromagnetic and antiferromagnetic couplings can also be observed but not simultaneously in a single sample. The sign of the coupling depends on the treatment of the sample.

In Ca-depleted samples, good simulations can be obtained for the three highest frequencies with a small distribution in J. At 9 GHz, however, the splitting obtained was too big compared to the experimental data and a rather large distribution was necessary to fit the data at all frequencies. The need for distribution has been routinely reported for simulations of coupled radical−metal center signal in protein.[31,34−36] The distribution in the exchange coupling is likely to reflect the distribution in protein conformation. In studies of protein conformational substates[37,38] the protein is modeled as a glass and a distribution of stuctural states (so-called substates) is used, each one being separated from the other by a small energy barrier. In solution, the interconversion between all of the substates is very fast and the protein conformation is the average of all the substates. As the temperature is lowered to trap the $S_2Y_Z^\bullet$ state, each protein is frozen in its own structural substate which can be different from its neighbors.

There are at least two possible explanations for the sign difference in the spin−spin coupling observed for the acetate- and calcium-treated samples. First, the differences in observed effective coupling constant may reflect differences in one or more of the four couplings between the radical and each manganese ion (eq 5). To understand better how this might arise, we consider a simple "dimer-of-dimers" model of the type recently analyzed by Blondin and co-workers.[39] In this model, the four-manganese cluster is characterized by three exchange couplings: one coupling between the metal ions for each dimer and a third between the two dimers. One of the dimers is composed of a Mn(III) and a Mn(IV) ion and the other two Mn(IV) ions. For a configuration where both dimers are antiferromagnetically coupled, the contribution from the two Mn(IV) dimer is zero and the effective coupling between a radical and such a cluster is given by $J_{III} - 1/2J_{IV}$. In this case, one possibility is that the spin coupling in one type of sample is characterized by a radical−Mn(III) coupling while in the other by a radical−Mn(IV) coupling. This naturally leads to a change in sign and magnitude of the effective coupling, even when the sign and magnitude of the intrinsic coupling remain constant.

An alternative possible source of the sign difference is that the K_i coefficients themselves have changed due to alterations in the electronic structure of the cluster. This possibility is interesting in light of the fact that the acetate-treated samples exhibit no multiline signal in the S_2 state while a multiline signal is readily observed for Ca-depleted samples. The fact that an underlying multiline-type signal is observed in the acetate-treated sample upon formation of the $S_2Y_Z^\bullet$ state is further evidence that the electronic structure of the manganese cluster undergoes significant modification. If the structure of the manganese cluster is different in the two types of samples, it would seem reasonable that the individual intrinsic exchange couplings between the metal centers and the radical will also be different. Undoubtedly, there is insufficient information from our experiments to distinguish between any of these various possibilities. However, as the signs of the exchange couplings are different, this necessarily implies that the spin pairs that give rise to the split signal in Ca-depleted and acetate-treated samples are distinct. The differences must arise from modifications in either the structure of the manganese cluster or the electronic interactions

between the interacting spins or both. Hence, any attempts to compare the two systems must necessarily account for these differences.

One of the interesting aspects of studying coupled systems is the possibility of deriving a distance between the two interacting species from the dipolar part of the interaction.[5a,14−18] In these studies, as in the present work, the point dipole approximation was used. However, as discussed above, the dipolar coupling is also an effective parameter depending strongly on the electronic structure of the two interacting centers and therefore not necessarily axial. It has been pointed out by Fournel and co-workers[36] that in more detailed treatments taking this fact into account it is not possible to extract structural information due to the inability to separate exchange and dipolar terms. Hence, for PS II the distances obtained from the simulations are *effective spin−spin* distances. There is not enough information to calculate an accurate geometrical distance between the radical and the manganese cluster. However, the very need to consider local spin distributions implies that the two species must be in proximity. It is clear that the simple approach which we have taken in conjunction with multifrequency high-field EPR can be useful in characterizing large changes in the coupling which makes it possible to detect changes in the structure of the tyrosyl−manganese cluster pair.

Conclusion

This study demonstrates the importance of using a multifrequency approach to analyze spin−spin coupling interactions, in particular high-field EPR. The application of high-field EPR enabled us to directly assign the sign of the spin−spin coupling. Using a simple spin coupling model, we simulated spectra obtained at four different frequencies to obtain good estimates of the coupling parameters and to verify the sign of the couplings. In the case of the calcium-depleted samples, this multifrequency approach also indicated the presence of distributed spin interactions. The details of the quantum mechanics leading to the observed distribution and sign difference are not completely understood. Future studies will need to focus on the importance of these differences and their structural and electronic implications for the tyrosyl−manganese cluster system.[40]

Acknowledgment. Moritz Knüpling is acknowledged for help in designing and building the high-field EPR spectrometer. We thank Anabella Ivancich for stimulating discussions. This research was supported by a grant from the Human Frontiers Science Organization (contract # RGO349) and by the E.U. through HCM grant FMRX-CT98-0214. P.D. acknowledges the CEA for a fellowship.

Supporting Information Available: Derivation of the energy levels and wave functions for two coupled $S = 1/2$ spins with hyperfine coupling. 3 GHz spectrum of the $S_2Y_Z^{\bullet}$ state in Ca-depleted PS II preparation. Calculated spectra for acetate-treated samples comparing ferromagnetic and antiferromagnetic couplings. Comparison between simulated spectra calculated by using the full hyperfine term or by using a binomial distribution to account for the hyperfine term of the manganese cluster. This material is available free of charge via the Internet at http://pubs.acs.org.

References and Notes

(1) (a) Rutherford, A. W.; Zimmermann, J.-L.; Boussac, A. In *The Photosystems: Structure, Function and Molecular Biology*; Barber, J., Ed.; Elsevier: Amsterdam, 1992; Chapter 5. (b) Britt, R. D. In *Oxygenic Photosynthesis: The Light Reactions*; Ort, D. R., Yocum, C. F., Eds; Kluwer Academic Publishers: Dordrecht, 1996; pp 137−164. (c) Diner, B. A.; Babcock, G. T. In *Oxygenic Photosynthesis: The Light Reactions*; Ort, D. R.; Yocum, C. F., Eds; Kluwer Academic Publishers: Dordrecht, 1996; pp 213−247.

(2) (a) Hoganson, C. W.; Babcock, G. T. *Science* **1997**, *277*, 1953. (b) Tommos, C.; Babcock, G. T. *Acc. Chem. Res.* **1998**, *31*, 18.

(3) Kok, B.; Forbush, B.; McGloin, M. *Photochem. Photobiol.* **1970**, *11*, 457.

(4) Dismukes, G. C.; Siderer, Y. *Proc. Natl. Acad. Sci. U.S.A.* **1981**, *78*, 274.

(5) (a) Rutherford, A. W.; Boussac, A. In *Research in Photosynthesis*; Murata, N., Ed; Kluwer Academic Publishers: Dordrecht, 1992; Vol. II, pp 21−27. (b) Debus, R. J. *Biochim. Biophys. Acta* **1992**, *1102*, 269. (c) Coleman, W. J. *Photosynth. Res.* **1990**, *23*, 1. (d) Yocum, C. F. *Biochim. Biophys. Acta* **1991**, *1059*, 1.

(6) Boussac, A.; Zimmermann, J.-L.; Rutherford, A. W. *Biochemistry* **1989**, *28*, 8984.

(7) MacLachlan, D. J.; Nugent, J. H. A. *Biochemistry* **1993**, *32*, 9772.

(8) (a) Sinclair, J. *Biochim. Biophys. Acta* **1984**, *764*, 247. (b) Sandusky, P. O.; Yocum, C. F. *Biochim. Biophys. Acta* **1986**, *849*, 85. (c) Gerken, S.; Dekker, J. P.; Schlodder, E.; Witt, H. T. *Biochim. Biophys. Acta* **1989**, *977*, 52. (d) Kühne, H.; Szalai, V. A.; Brudvig, G. W. *Biochemistry* **1999**, *38*, 6604.

(9) (a) Boussac, A.; Sétif, P.; Rutherford, A. W. *Biochemistry* **1992**, *31*, 1224. (b) Andréasson, L. E.; Lindberg, K. *Biochim. Biophys. Acta* **1992**, *1100*, 177. (c) Ono, T.; Inoue, Y *Biochim. Biophys. Acta* **1990**, *1020*, 269.

(10) Boussac, A.; Zimmermann, J.-L.; Rutherford, A. W.; Lavergne, J. *Nature* **1990**, *347*, 303.

(11) (a) Hallahan, B. J.; Nugent, J. H. A.; Warden, J. T.; Evans, M. C. W. *Biochemistry* **1992**, *31*, 4562. (b) Boussac, A.; Rutherford, A. W. *Biochemistry* **1992**, *31*, 7441.

(12) Gilchrist, M. L.; Ball, J. A.; Randall, D. W.; Britt, R. D. *Proc. Natl. Acad. Sci. U.S.A.* **1995**, *92*, 9545.

(13) Tang, X. S.; Randall, D. W.; Force, D. A.; Diner, B. A.; Britt, R. D. *J. Am. Chem. Soc.* **1996**, *118*, 7638.

(14) MacLachlan, D. J.; Nugent, J. H. A.; Warden, J. T.; Evans, M. C. W. *Biochim. Biophys. Acta* **1994**, *1188*, 325.

(15) Force, D. A.; Randall, D. W.; Britt, R. D. *Biochemistry* **1997**, *36*, 12062.

(16) Peloquin, J. M.; Campbell, K. A.; Britt, R. D. *J. Am. Chem. Soc.* **1998**, *120*, 6840.

(17) Dorlet, P.; Di Valentin, M.; Babcock, G. T.; McCracken, J. L. *J. Phys. Chem. B* **1998**, *102*, 8239.

(18) Lakshmi, K. V.; Eaton, S. S.; Eaton, G. R.; Frank, H. A.; Brudvig, G. W. *J. Phys. Chem. B* **1998**, *102*, 8327.

(19) (a) Berthold, D. A.; Babcock, G. T.; Yocum, C. F. *FEBS Lett.* **1981**, *277*, 69. (b) Ghanotakis, D. F.; Topper, J.; Babcock, G. T.; Yocum, C. F. *Biochim. Biophys. Acta* **1984**, *767*, 524.

(20) Mishra, R. K.; Ghanotakis, D. F. *Photosynth. Res.* **1994**, *42*, 37.

(21) Muller, F.; Hopkins, M. A.; Coron, N.; Grynberg, M.; Brunel, L.; Martinez, G. *Rev. Sci. Instrum.* **1989**, *60*, 3681.

(22) Press, W. H.; Flannery, B. P.; Teukolsky, S. A.; Vetterling, W. T. *Numerical Recipes*; Cambridge University Press: New York, 1986.

(23) (a) Smith, T. D.; Pilbrow, J. R. *Coord. Chem. Rev.* **1974**, *13*, 173. (b) Eaton, S. S.; More, K. M.; Sawant, B. M.; Boymel, P. M.; Eaton, G. R. *J. Magn. Res.* **1983**, *52*, 435. (c) Hore, P. J. In *Advanced EPR: Applications in Biology and Biochemistry*; Hoff, A. J., Ed.; Elsevier: Amsterdam, 1989; Chapter 12.

(24) Hoganson, C. W.; Babcock, G. T. *Biochemistry* **1988**, *27*, 5848.

(25) The Heisenberg exchange Hamiltonian is given in eq 5. The coefficients C_{ZZ} and $C_{\pm}$ expand as follow in function of J and D: $C_{ZZ} = -J - 2D(\cos^2\Theta - 1/3)$ and $C_{\pm} = -(J + D(\cos^2\Theta - 1/3))/2$ where Θ is the angle between the magnetic field and the axis joining the two point dipoles.

(26) Bertrand, P.; More, C.; Guigliarelli, B.; Fournel, A.; Bennet, B.; Howes, B. *J. Am. Chem. Soc.* **1994**, *116*, 3078.

(27) Bertrand, P.; Camensuli, P.; More, C.; Guigliarelli, B. *J. Am. Chem. Soc.* **1996**, *118*, 1426.

(28) Un, S.; Brunel, L.-C.; Brill, T.; Zimmermann, J.-L.; Rutherford, A. W. *Proc. Natl. Acad. Sci. U.S.A.* **1994**, *91*, 5262.

(29) Un, S.; Tang, X.-S.; Diner, B. A. *Biochemistry* **1996**, *35*, 679.

(30) Un, S.; Atta, M.; Fontecave, M.; Rutherford, A. W. *J. Am. Chem. Soc.* **1995**, *117*, 10713.

(31) Houseman, A. L. P.; Doan, P. E.; Goodin, D. B.; Hoffman, B. M. *Biochemistry* **1993**, *32*, 4430.

(32) Benecky, M. J.; Frew, J. E.; Scowen, N.; Jones, P.; Hoffman, B. M. *Biochemistry* **1993**, *32*, 11929.

(33) Patterson, W. R.; Poulos, T. L.; Goodin, D. B. *Biochemistry* **1995**, *34*, 4342.

(34) Stevenson, R. C.; Dunham, W. R.; Sands, R. H.; Singer, T. P.; Beinert, H. *Biochim. Biophys. Acta* **1986**, *869*, 81.

(35) Rutter, R.; Valentine, M.; Hendrich, M. P.; Hager, L. P.; Debrunner, P. G. *Biochemistry* **1983**, *22*, 4769.

(36) Fournel, A.; Gambarelli, S.; Guigliarelli, B.; More, C.; Asso, M.; Chouteau, G.; Hille, R.; Bertrand, P. *J. Chem. Phys.* **1998**, *109*, 10905.

(37) Frauenfelder, H.; Sligar, S. G.; Wolynes, P. G. *Science* **1991**, *254*, 1598.

(38) Stein, D. In *Protein Structure: Molecular and Electronic Reactivity*; Springer-Verlag: New York, 1987; pp 85−93.

(39) Blondin, G.; Davydov, R.; Philouze, C.; Charlot, M.-F.; Styring, S.; Åkermark, B.; Girerd, J.-J.; Boussac, A. *J. Chem. Soc., Dalton Trans.* **1997**, *21*, 4069.

(40) A very recent 9 GHz EPR study of the $S_2Y_Z^{\bullet}$ state in oriented PS II membranes[41] appeared while this paper was under review. In this orientation study, the starting parameters for the coupling between the radical and the metal cluster were taken from ref 18 in which the exchange coupling was taken to be antiferromagnetic on the basis of simulations of 9 GHz EPR data. In particular, the sign of the exchange coupling is referred to during the analysis to determine the angle θ_D between the interspin vector and the normal to the membrane which is a key factor in the simulations. Our data show that the coupling in acetate-treated samples is in fact ferromagnetic and this may influence the simulations of oriented data and their resulting interpretation.

(41) Lakshmi, K. V.; Eaton, S. S.; Eaton, G. R.; Brudvig G. W. *Biochemistry* **1999**, *38*, 12758.